AIAA AVIATION Forum
June 25-29, 2018, Atlanta, Georgia
2018 AIAA/CEAS Aeroacoustics Conference

10.2514/6.2018-3941

Check for updates

Modelling Noise Sources in Offset Two-Stream Jets Using Linear Stability Theory

Nikhil Sohoni* and Aniruddha Sinha†

Dept. of Aerospace Engineering, Indian Institute of Technology Bombay, Mumbai 400076, INDIA

Two-stream jets with a low-speed secondary stream are significantly quieter than high-speed single-stream jets. Further noise reduction in the critical downward sector has been obtained in experiments by offsetting the secondary jet downwards relative to the primary jet, both their axes being horizontal. Here, we report on a computationally-efficient model of such offset-driven modification of the noise sources in two-stream jets. We begin by proposing a consistent model of the three-dimensional turbulent mean velocity field for jets of varying offsets; this is based on fitting sparse two-dimensional experimental data reported by Murakami and Papamoschou (AIAA Journal, 40(6), 1131–37, 2002). The noise sources are subsequently modelled as wavepackets derived from quasi-parallel linear bi-global stability theory applied to the turbulent mean flow field. Our results indicate that the so-called 'inner modes' associated with the inner shear layer of the two-stream jet are indeed weakened in the bottom sector due to the offset. On the other hand, 'outer modes' linked to the weaker outer shear layer display some enhancement in the same sector. Overall, the model accords with noise modifications observed in experiments.

Downloaded by Aniruddha Sinha on June 28, 2018 | http://arc.aiaa.org | DOI: 10.2514/6.2018-3941

I. Introduction

Two-stream coaxial jets are exemplified by the high-bypass ratio jet engines currently deployed in civil aviation. The low-speed colder secondary stream surrounding the high-speed hot core jet not only improves the overall cycle efficiency of the engine but also leads to reduced jet mixing noise. The bypass stream lowers the effective jet velocity necessary to achieve a given amount of thrust. Since the aerodynamic noise scales as a high power of the effective jet velocity (between six and eight, for Mach numbers ranging from low subsonic to moderate supersonic)[1] whereas the scaling with effective area is linear, high bypass is a very efficient way of decreasing the radiated jet noise. The aeroacoustics of two-stream jets have been studied in detail in the recent past[2–4].

Bypass ratios as high as ten are commonly used in jet engines now, tremendously increasing the overall jet diameter required to generate the required thrust. Thus, further increase of bypass ratio appears infeasible, and researchers are exploring other avenues for the continued reduction in jet noise demanded by aviation regulations. One such line of enquiry has focused on preferentially shielding the bottom sector of the jet where exposure to ground personnel and built structures is maximum. The goal is to redirect the noise to sectors where it is least harmful while having the minimal effect on engine thrust.

Initial investigations explored modifications to the azimuthal directivity of the bypass stream to thicken the shear layer below the jet. Three approaches were taken: offsetting the two jets parallel to each other[5], tilting the axis of the secondary stream slightly with respect to that of the core stream[6], and installing wedges or vanes in the secondary stream outlet to direct it to the bottom half[7]. The last method is the easiest to implement in deployed configurations. Investigations of various design concepts for this method indicated that the acoustic benefit tends to be significant at low bypass ratios and low flight speeds, but diminishes at higher values of both these parameters[8].

A more recent line of exploration has investigated the feasibility of keeping the bypass stream undisturbed but adding a low-speed offset tertiary stream, again preferentially shrouding the bottom part of the engine[9–13]. Since the tertiary stream carries very little momentum, the distortion of thrust is minimal.

*PhD Student
†Assistant Professor; AIAA Member; Corresponding author: as@aero.iitb.ac.in

Copyright © 2018 by Nikhil Sohoni and Aniruddha Sinha. Published by the American Institute of Aeronautics and Astronautics, Inc., with permission.

The concepts discussed above have mainly been investigated experimentally. Reynolds-averaged Navier Stokes (RANS) simulations have been pursued to support experiment design and develop insight into differences in mean flow development with proposed modifications to the two or three-stream jets [14–16]. Acoustic-analogy based noise modelling using RANS solutions has a long history in single-stream jets, and efforts have been made recently to extend the approach to the complex multi-stream jets under discussion here [11,17].

In this paper, we start on an alternate computationally-efficient path to modelling the noise sources in offset multi-stream jets based on the theory of wavepackets. The latter refer to the spatially growing, saturating and decaying signatures observed most prominently in the hydrodynamic pressure field near the jet, which are coherent over regions significantly larger than the characteristic length of the flow. Owing to their high coherence, wavepackets are responsible for a large component of the jet mixing noise that radiates to the far field, primarily in the louder aft sector [18].

Wavepackets were first observed experimentally in jets by Mollo-Christensen [19]. Soon after, researchers noted their similarity to the linear Kelvin-Helmholtz (K-H) instability waves supported by the time-averaged flow field of the turbulent jet, and started modelling them as such [20,21]. With recent advances in experimental sophistication and large-eddy simulation of high Reynolds number jets, this modelling approach has been validated at length, and found to be quite accurate for single-stream jets [22–24]. Stability models for both quasi-parallel flow (linear stability theory, LST) and slowly-varying flow (parabolized stability equations, PSE) have been used in this regard.

LST of coaxial jets has also been pursued for some time now [25–28], although direct validation of results against experiments or LES data has been lacking. Recently, PSE has been used to model wavepackets in the slowly-varying coaxial jet mean flow; comparison of predicted wavepackets against those educed from LES data appears encouraging [29].

The spatial LST study of coaxial jets [26,27] identified two separate unstable K-H modes for each pair of frequency and azimuthal Fourier mode of perturbation; this is unlike the single K-H instability that appears in single-stream round jets. The two modes were found to be associated with the inner and outer shear layers respectively, and were termed 'inner mode' and 'outer mode'. Of course, such a distinction is only possible prior to the close of the outer potential core, beyond which the modes may be supposed to merge.

We hypothesize that the acoustic benefit of offsetting the two streams of a jet derives due to the reduced instability of K-H modes (inner and/or outer) and their favourable azimuthal asymmetry in the modified flow. In the present study, we explore this using bi-global spatial LST. Subsequently, we can use PSE or the improved one-way spatial integration method [30] to refine the model.

II. Mean flow model for offset two-stream jets

Murakami and Papamoschou [5] have presented a detailed description of the time-averaged (mean) axial velocity in several coaxial and eccentric (i.e., completely offset) two-stream laboratory jets. In their experiments, the primary (inner) nozzle had exit diameter $D_p = 12.7$ mm and was designed for an exit Mach number of 1.5 using the method of characteristics for ideal expansion; its Reynolds number was 5.5×10^5. The secondary (outer) nozzle had several designs, with different exit diameters, D_s; moreover these were run at several subsonic Mach numbers. The stagnation temperature for both nozzles was the ambient, and the two nozzle exits were in the same plane. To create a mean flow model, we have chosen the concentric 'C17M90' and the corresponding eccentric 'E17M90' cases among the configurations that they reported. These jets had $D_s/D_p = 1.7$, and the secondary Mach number was 0.9. In the eccentric case, the secondary nozzle was offset downwards such that it was touching the primary nozzle at the top, leaving no air gap in between. Apart from E17M90, the only other eccentric jet whose mean velocity field was reported in Ref. 5 was E14M90 having $D_s/D_p = 1.4$ and the same secondary jet Mach number.

In the following, all length dimensions will be implicitly normalized by D_p, and all velocities by the primary nozzle exit velocity U_p (430 m/s in the reference). The profiles of the mean axial velocity (denoted $\overline{u}$) for the C17M90 and E17M90 cases at several x stations presented in Ref. 5 are reproduced in fig. 1a.

We fitted these mean velocity profiles with an offset double truncated-Gaussian function as described below; a single truncated-Gaussian function has been in long usage for modelling round single-stream jet velocity profiles [21,31]:

Downloaded by Aniruddha Sinha on June 28, 2018 | http://arc.aiaa.org | DOI: 10.2514/6.2018-3941

Downloaded by Aniruddha Sinha on June 28, 2018 | http://arc.aiaa.org | DOI: 10.2514/6.2018-3941

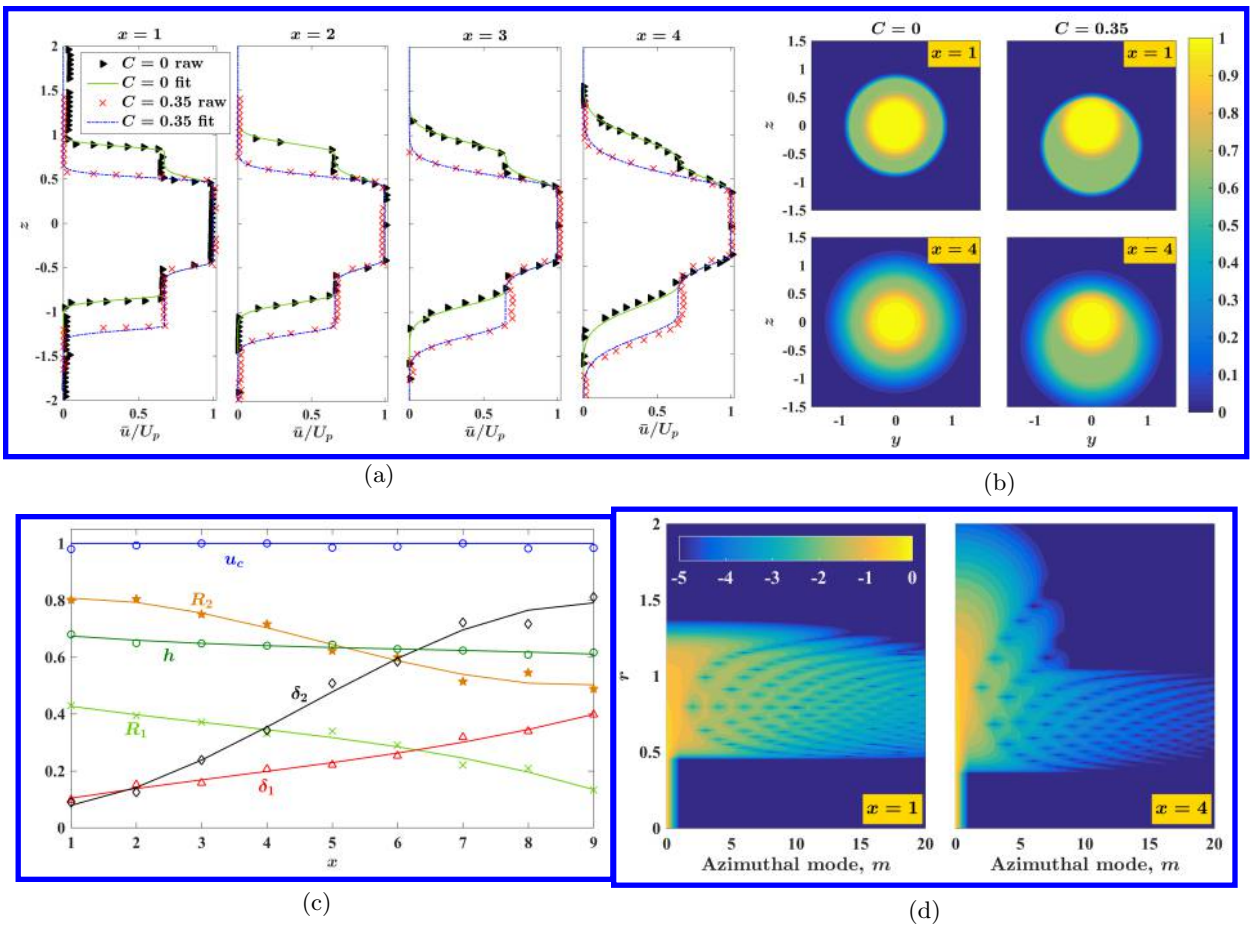

(a) (b) (c) (d)

Figure 1: (a) Mean axial velocity profiles of C17M90 and E17M90 jets from Ref. 5 fitted with the function in eqn. (1). (b) Contours of mean axial velocity ($\bar{u}/U_p$) for the two jets at two x-stations. (c) The parameters of the fitting function of eqn. (1), smoothed by cubic splines. (d) Log absolute values of the azimuthal Fourier modes of mean velocity field $\breve{\bar{u}}_m$ (normalized by their maxima) in the $C = 0.35$ offset jet at $x = 1$ and 4.

$$
\begin{aligned}
\overline{u}(x,y,z) &= u_c(x)\left\{(1-h(x))\overline{u}_1(x,y,z) + h(x)\overline{u}_2(x,y,z)\right\},\\
\overline{u}_k(x,y,z) &= \begin{cases} 1, & \text{if } \sigma_k(y,z) < R_k(x),\\ \exp\left(-\dfrac{(\sigma_k(y,z)-R_k(x))^2}{\delta_k^2(x)}\right), & \text{otherwise,}\end{cases} \qquad k \in \{1,2\},\\
\sigma_1(y,z) &:= \sqrt{y^2+z^2}, \qquad \sigma_2(y,z) := \sqrt{y^2+(z+C)^2}.
\end{aligned}
\tag{1}
$$

Here, R_1 and R_2 locate the inner edges of the inner and outer shear layers respectively, δ_1 and δ_2 are related to their respective thicknesses, h represents the ratio of the secondary to primary nozzle exit velocities, and u_c corresponds to the centerline velocity; all these parameters are functions of the streamwise coordinate x. The primary jet is modelled by $\overline{u}_1$; note that it is concentric with the x-axis. To model a consistent offset of the secondary jet (modelled by $\overline{u}_2$) in the z-direction relative to the primary jet, we introduce the parameter C; note that it is a constant applicable uniformly to all x stations of a jet. A positive value of C will model a downward offset of the secondary jet, with z-axis pointing vertically up. The function introduced here allows us to model the three-dimensional mean velocity field in dual-stream jets with arbitrary offset, assuming that the two streams evolve independently.

Figure 1a demonstrates that this function is a good fit for the velocity profiles across a range of x-stations uniformly for the C17M90 coaxial jet and the E17M90 eccentric jet. A least-squares fitting was

used to determine the optimal parameter values jointly from the two jets at each x-station, so that the only parameter that differed between the two cases was the offset C. For the coaxial jet, it is obvious that C must be 0. Since the nozzle diameter ratio is 1.7, the value of $C = 0.35$ may be deduced for the fully-offset E17M90 jet. Our model then allows us to simulate the mean velocity in the entire $y - z$ plane for arbitrary choice of C. Results from this exercise are presented in fig. 1b. Note that the secondary jet is offset downwards (towards negative z); this same orientation will be used consistently in the remainder of the paper.

The streamwise evolution of the parameters of the fitting function is presented in fig. 1c. The primary potential core for this jet extends to $10D_p$ (R_1 is seen to be approaching zero by $x = 9$), and the parameters are seen to vary smoothly up to this point. The cubic spline fits to these parameter values, as shown in the figure, may be used to model the jet at intermediate axial stations.

In the coaxial round jet, the linear stability analysis is most convenient in polar coordinates (r, θ), owing to decoupling of Fourier azimuthal modes. It will be shown in the next section that such decoupling is not possible for the offset jet. However, for ease of comparison of stability results between coaxial and offset jets, the LST will be pursued in polar coordinates for the latter case too. In view of this, we expand the mean axial velocity in terms of its azimuthal Fourier modes in the usual fashion:

$$\overline{u}\,(x, r, \theta) = \sum_{m=-\infty}^{\infty} \breve{\overline{u}}_m\,(x, r)\,\mathrm{e}^{\iota m\theta}, \tag{2}$$

where $\breve{\overline{u}}_m$ is the mth azimuthal Fourier mode of $\overline{u}$, and ι is the square root of negative unity. Owing to the mirror symmetry of the offset jet mean flow field about $y = 0$, it is straightforward to show that the negative and positive azimuthal modes are identical (and both are real) if θ is defined with reference to the z axis.

Figure 1d demonstrates that the azimuthal complexity of the eccentric jet mean flow field under consideration (with $C = 0.35$) at $x = 1$ and 4 is limited. In particular, azimuthal Fourier modes beyond $m = \pm 15$ are more than three orders of magnitude lower than the most dominant one ($m = 0$). Moreover, the offset of the secondary jet clearly manifests in azimuthal complexity in a limited radial domain around the nominal location of the secondary shear layer ($r \approx 0.85$) at $x = 1$, with some spreading further downstream at $x = 4$. We denote the maximum non-negligible azimuthal mode of the mean flow field as M. The stippled nature of the contour plots is due to increasing number of zero-crossings of $\breve{\overline{u}}_m$ as m increases.

In the subsequent LST, we use the parallel flow approximation to assume that the other components of the mean velocity field (viz. radial and azimuthal) are negligible. The mean temperature (or equivalently mean density) measurement was not reported in Ref. 5; in the present work we assume it to be the ambient temperature everywhere (isothermal jet approximation), even though the actual jets were cold (the stagnation temperature was the ambient value).

III. Linear stability theory for offset multi-stream jets

As discussed in the preceding section, the only symmetry in the mean flow field of offset multi-stream jets is mirror symmetry about the plane joining the axes of the two streams. For the purpose of applying LST, the axial variation of the mean flow is neglected. The remaining stability problem is bi-global where there are two inhomogeneous directions: viz. $y - z$ or $r - \theta$. The latter formulation is preferred here since it connects well with the analysis for coaxial jets.

The flow field of the jet is described in cylindrical coordinates $\boldsymbol{x} = (x, r, \theta)$ by $\boldsymbol{q} = (u, v, w, p, \zeta)^{\mathrm{T}}$, which respectively denote the axial, radial and azimuthal components of velocity, pressure, and specific volume. LST starts by decomposing $\boldsymbol{q}$ into a time-invariant base flow (herein the turbulent mean flow) $\overline{\boldsymbol{q}}$, and the residual fluctuations $\boldsymbol{q}'$. The set of five non-dimensional governing equations for the latter in the viscous compressible flow linearized about $\overline{\boldsymbol{q}}$ are compactly represented in matrix form as

$$\left\{\overline{\mathscr{L}}^0 + \overline{\mathscr{L}}^t \frac{\partial}{\partial t} + \overline{\mathscr{L}}^x \frac{\partial}{\partial x} + \overline{\mathscr{L}}^r \frac{\partial}{\partial r} + \overline{\mathscr{L}}^\theta \frac{\partial}{\partial \theta} + \sum_{\zeta,\tau\in\{x,r,\theta\}} \overline{\mathscr{L}}^{\zeta\tau} \frac{\partial^2}{\partial\zeta\partial\tau}\right\}\boldsymbol{q}' = \boldsymbol{0}. \tag{3}$$

The 5×5 coefficient matrices $\overline{\mathscr{L}}$ are linear functions of the mean flow field $\overline{\boldsymbol{q}}$, except for the constant $\overline{\mathscr{L}}^t$.

Since the $\overline{\mathscr{L}}$'s are time-invariant and independent of x due to the corresponding properties of $\overline{\boldsymbol{q}}$, the solution is separable into its frequency components and axial wavenumbers (normal modes). In spatial LST, we allow the latter to be complex to model the growth/decay of the modes with x. With this, the LST ansatz for $\boldsymbol{q}'$ is

Downloaded by Aniruddha Sinha on June 28, 2018 | http://arc.aiaa.org | DOI: 10.2514/6.2018-3941

$$\boldsymbol{q}'(\boldsymbol{x},t) = \hat{\boldsymbol{q}}_\omega(r,\theta)\,\mathrm{e}^{\iota(\alpha x-\omega t)} + \text{c.c.}, \qquad \hat{\boldsymbol{q}}_\omega(r,\theta) = \sum_{m=-\infty}^{\infty} \tilde{\boldsymbol{q}}_{\omega,m}(r)\,\mathrm{e}^{\iota m\theta}. \tag{4}$$

Here, m is the Fourier azimuthal mode as before. The real frequency ω will be reported subsequently in terms of the Strouhal number $St := \omega D_p/(2\pi U_p)$. Further, $\tilde{\boldsymbol{q}}_{\omega,m}$ is the mode shape function and α is its complex axial wavenumber. The real and imaginary parts of α, denoted α_r and α_i, respectively signify the wavenumber and the negative of the growth rate (decay rate).

Substituting the foregoing ansatz in the linearized governing equation, using the azimuthal Fourier decomposition of the matrices $\overline{\mathscr{L}}$ analogous to eqn. (2), and taking the azimuthal Fourier transform of the resulting equation for an arbitrary azimuthal Fourier mode n obtains, after simplification, the following

$$\begin{aligned} -\iota\omega\breve{\overline{\mathscr{L}}}^{t}\tilde{\boldsymbol{q}}_{\omega,n} + \sum_{m=-M}^{M}\Bigg[\Bigg\{\breve{\overline{\mathscr{L}}}^{0}_{m} + \breve{\overline{\mathscr{L}}}^{r}_{m}\frac{\partial}{\partial r} + \breve{\overline{\mathscr{L}}}^{rr}_{m}\frac{\partial^2}{\partial r^2} + \iota(n-m)\left(\breve{\overline{\mathscr{L}}}^{\theta}_{m} + \breve{\overline{\mathscr{L}}}^{r\theta}_{m}\frac{\partial}{\partial r}\right) - (n-m)^2\breve{\overline{\mathscr{L}}}^{\theta\theta}_{m}\Bigg\} \\ +\iota\alpha\left\{\breve{\overline{\mathscr{L}}}^{x}_{m} + \breve{\overline{\mathscr{L}}}^{xr}_{m}\frac{\partial}{\partial r} + \iota(n-m)\breve{\overline{\mathscr{L}}}^{\theta x}_{m}\right\} - \alpha^2\left\{\breve{\overline{\mathscr{L}}}^{xx}_{m}\right\}\Bigg]\tilde{\boldsymbol{q}}_{\omega,n-m} = \boldsymbol{0}. \end{aligned} \tag{5}$$

Here, $\breve{\overline{\mathscr{L}}}_m$ is the mth azimuthal Fourier mode of the corresponding $\overline{\mathscr{L}}$, and it inherits the azimuthal complexity of $\overline{\boldsymbol{q}}$ so that m is limited to $\pm M$. The last term in braces, which multiplies α^2, is usually negligible at the high Reynolds numbers considered[32,33].

Equation (5) indicates that the nth azimuthal mode of the solution $\tilde{\boldsymbol{q}}$ is coupled with other azimuthal modes in the set $[n-M, n+M]$. However, the $(n+1)$th mode of the solution is coupled to modes in the set $[n-M+1, n+M+1]$. Thus, by induction, all azimuthal modes are coupled to each other. This is to be expected since the problem is one of bi-global stability, and azimuthal Fourier transform cannot modify this fundamental characteristic. However, just like the limited azimuthal complexity possessed by the mean flow field, the fluctuations will also have negligible contributions from higher-order azimuthal modes, say those beyond $\pm N$. This is analogous to placing a limit to the resolution of the physical azimuthal domain in a discretized implementation of the bi-global stability calculation in the (r,θ) plane. The resulting system of equations (with the neglect of the α^2 term) is a generalized linear eigenvalue problem for the pair $(\alpha_\omega, \{\tilde{\boldsymbol{q}}_{\omega,n}\}_{n=-N}^{N})$, where we have made explicit the dependence of the eigenvalue α on ω.

For ease of visualization, the eigenfunctions are presented in the (r,θ) domain as $\hat{\boldsymbol{q}}_\omega$ instead of as $\{\tilde{\boldsymbol{q}}_{\omega,n}\}_{n=-N}^{N}$ (see eqn. (4) for the distinction). In the coaxial jet, the LST eigensolutions for a given ω are readily categorized as modes of azimuthal character consistent with $m = 0$, 1, 2, etc., since the azimuthal Fourier modes are independent. For a multi-stream jet with a small offset, each LST eigensolution for a given ω is still dominated by a single m, although it also exhibits partial character of all other azimuthal modes. We introduce the nomenclature $\mu = 0$ to denote the eigensolutions dominated by $m = 0$, $\mu = 1$ to denote those dominated by $m = 1$, and so on. As the offset increases, one can still trace the evolution of a given μ mode, although the identification may become more ambiguous. We denote the eigenfunction for a particular μ mode as $\hat{\boldsymbol{q}}_{\omega,\mu}(r,\theta)$, and the corresponding eigenvalue as $\alpha_{\omega,\mu}$.

The usual boundary conditions apply to the centerline[34] and far-field[35] in the radial domain since the flow is axisymmetric at both limits. The radial grid is clustered in the shear layer and stretches out in the far field. Fourth-order central difference is used to discretize the radial derivative operators. The resulting sparse matrix eigenvalue problem is solved using the parallel implementation of the ARPACK library[36].

To account for the jet spread in the streamwise direction, LST eigenproblems are solved separately at several axial stations. From the set of eigensolutions at each station, the lowest order μ modes are determined. Subsequently, following Ref. 22, a single 'composite eigenfunction' valid across all these axial stations is calculated for each pair of ω and μ:

$$\hat{\boldsymbol{Q}}_{\omega,\mu}(x,r,\theta) = \hat{\boldsymbol{q}}_{\omega,\mu}(r,\theta;x)\exp\left[\iota\int_{x_0}^{x}\alpha_{\omega,\mu}(\xi)\mathrm{d}\xi\right]. \tag{6}$$

Prior to its usage here, $\hat{\boldsymbol{q}}_{\omega,\mu}$ is normalized such that it is unity (with no imaginary part) at the $(r,\theta=\theta_0)$ position where its complex amplitude is maximum; herer θ_0 refers to the azimuthal coordinate θ where all the eigenfunctions peak, and is an arbitrary but consistent choice. The normalization ensures that the wave-like behaviour (oscillation, and growth or decay) of the composite eigenfunction is determined solely by the complex wavenumber $\alpha_{\omega,\mu}(x)$, and not by the 'shape function' $\hat{\boldsymbol{q}}$. The first x-station where the LST eigenproblem is solved is denoted x_0.

Downloaded by Aniruddha Sinha on June 28, 2018 | http://arc.aiaa.org | DOI: 10.2514/6.2018-3941

IV. Results

We now present results from the LST calculations. For the jet mean flow field, we use various offsets in between $C = 0$ (coaxial) and $C = 0.35$ (fully eccentric). To understand the variation of stability characteristics with spreading of the jet, we perform LST at several x-stations. Examples of the mean flows 'manufactured' for this purpose, along with their Fourier azimuthal characteristics, have been presented in fig. 1. The pressure eigenfunctions are the most relevant for acoustics, and hence these are presented exclusively. The maximum number of azimuthal Fourier modes of the mean flow M and that of the solution N needed for convergence of the LST calculations are respectively 30 and 35, although most cases were converged with much fewer modes. The radial domain (limited to $r = 8.5$) is discretized with 800 grid points.

The LST calculations presented here are for $St = 0.1$ (referred to the primary jet). In the discussion of the results, it will be helpful to note that this corresponds to $St = 0.3$ referred to the secondary nozzle exit diameter and velocity. This St of 0.1 corresponds to a wavepacket with a very long wavelength ($\approx 8D_p$, as we will see), for which the parallel-flow assumption of LST may be questionable. However, we still chose this St so as to assure unstable modes at a sufficient number of x-stations for elucidating the evolution of wavepackets in offset dual-stream jets.

Figure 2 presents the inner eigensolutions from LST applied to dual-stream jets of varying eccentricity for $St = 0.1$ at $x = 1$ and 4. The first three azimuthal mode-dominant solutions (viz. $\mu = 0$, 1 and 2) are depicted, these being the most relevant for far-field acoustic radiation[37,38]. It will be recalled that the inner modes are associated with the inner shear layer. Indeed the corresponding eigenfunctions are seen to peak approximately at $r = 0.5$. Moreover, their phase Mach number $c_p := \omega/\alpha_r$ is approximately equal to the average Mach number of the inner shear layer.

We observe that the inner modes' eigenspectrum (growth rate and phase speed) is not affected significantly by the eccentricity of the jet, except for the case of $\mu = 2$ at $x = 4$. Having said that, very minor increases of growth rate may be seen in the case of $\mu = 0$ (at both x-stations), with corresponding minor decreases in the cases of $\mu = 1$ and 2. However, the major difference appears in the eigenfunctions' shapes. Starting from pure azimuthal Fourier mode structures ($m = 0$, 1 and 2 in the respective cases of $\mu = 0$, 1 and 2), the character remains approximately similar for the partial offset jet ($C = 0.15$). Whereas a minor strengthening of the $\mu = 0$ eigenfunction is discernible in the bottom (thicker) shear layer, a significant diminution is observed in the $\mu = 1$ and 2 cases at the bottom region. This may be related to the reduced acoustic radiation to the bottom sector in the offset dual-stream jets, a point that we will reinforce subsequently. The trend is magnified in the fully eccentric jet ($C = 0.35$). One also notices an approximate anti-node forming at the top of the jet with an approximate bisection of the lobe of the eigenfunction at the top of the shear layer, where the two nozzles touch each other and essentially pinch off the flow. There are no prominent differences in the inner eigenfunctions' structures between the two axial stations presented.

We now move on to the outer modes depicted in fig. 3. As the name suggests, these modes may be identified by their peak coinciding with the outer shear layer ($r \approx 0.85$) and phase speed being related to the average speed in that shear layer. Let us first consider the coaxial jet results. It may appear paradoxical that the outer modes have significantly higher growth rates compared to the inner modes at $x = 1$, even though the gradients are similar for both shear layers. This may be resolved by recalling that the $St = 0.1$ corresponds to $St = 0.3$ when normalized by the parameters of the secondary jet; growth rates typically peak around this Strouhal number. We also note that the outer modes' growth rates are rapidly diminished by $x = 4$.

Although the outer modes appear to be strongly unstable in the coaxial jet studied, we caution against emphasizing this. Due to the limitations of the mean velocity data published in Ref. 5, the jet studied here has a strong secondary jet (Mach 0.9) that is rare in jet engine applications. Instead, the secondary jet is typically much slower and spreads quicker, so that it is expected to be much more stable (e.g., see Ref. 29).

Turning now to the outer eigenspectra of the offset jets at $x = 1$, we note that the growth rate generally decreases appreciably with increasing offset, attended by an increase in phase speed in several cases. The differences in the growth rate with offset are much less at $x = 4$. In the eigenfunctions, we observe severe distortion of all three μ modes with increasing eccentricity. The distortion is very pronounced even for the $C = 0.15$ jet in the $\mu = 0$ mode, with the eigenfunction peaking in the top sector. The opposite effect is observed in the higher μ modes.

Having studied the variation of eigenspectra with varying offset in fig. 2 and 3, we now turn to an analysis of their variation with streamwise distance from the nozzle exit in fig. 4. As expected with the spreading

Downloaded by Aniruddha Sinha on June 28, 2018 | http://arc.aiaa.org | DOI: 10.2514/6.2018-3941

Downloaded by Aniruddha Sinha on June 28, 2018 | http://arc.aiaa.org | DOI: 10.2514/6.2018-3941

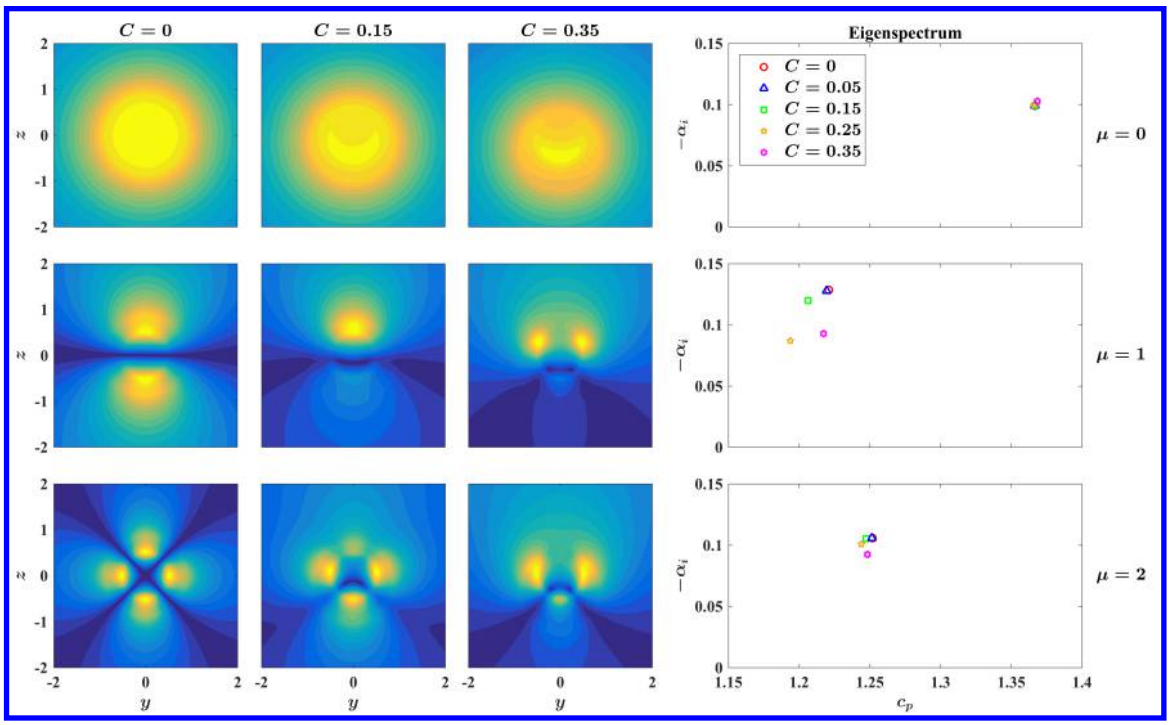

(a) Inner modes at $x = 1$.

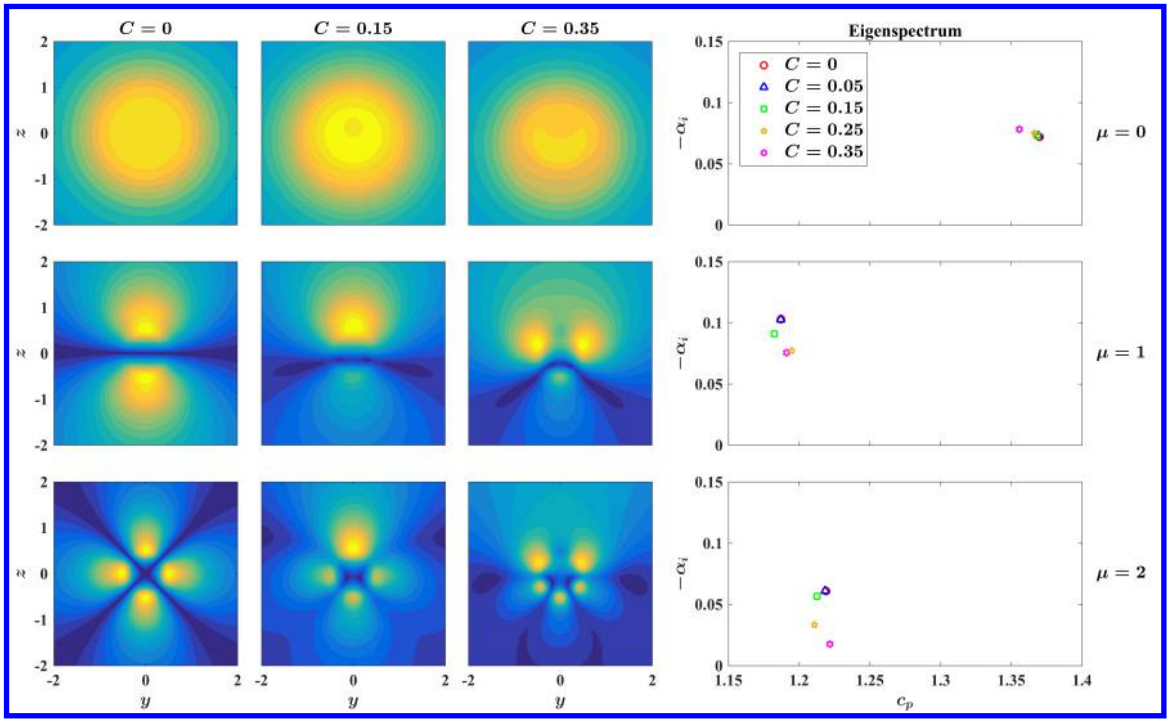

(b) Inner modes at $x = 4$.

Figure 2: Absolute pressure component of inner mode eigenfunctions (first three columns) and eigenvalues (last column) for $St = 0.1$ in jets at (a) $x = 1$ and (b) $x = 4$. Eigenfunctions are presented for the coaxial jet ($C = 0$), partial offset jet ($C = 0.15$), and fully eccentric jet ($C = 0.35$). Eigenspectra are shown for five jets with increasing C. At each x-station, results are presented row-wise for the first three μ modes. The orientation of the eigenfunction plots is such that the lower halves correspond to the thicker shear layer.

Downloaded by Aniruddha Sinha on June 28, 2018 | http://arc.aiaa.org | DOI: 10.2514/6.2018-3941

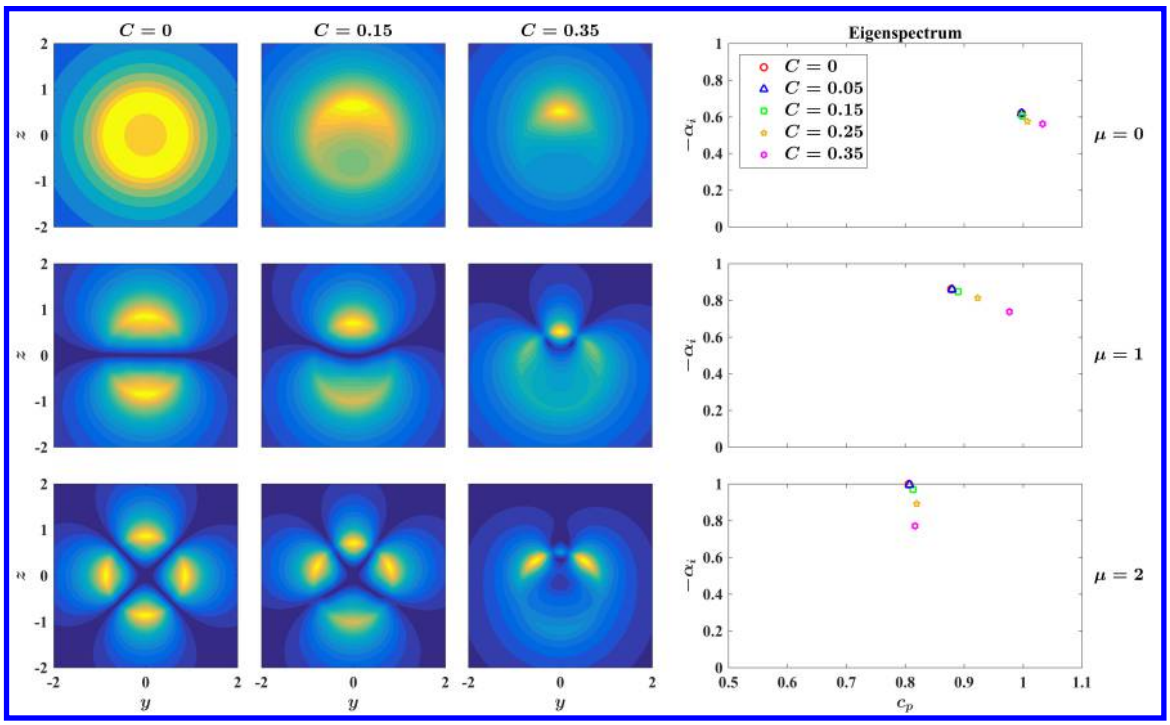

(a) Outer modes at $x = 1$.

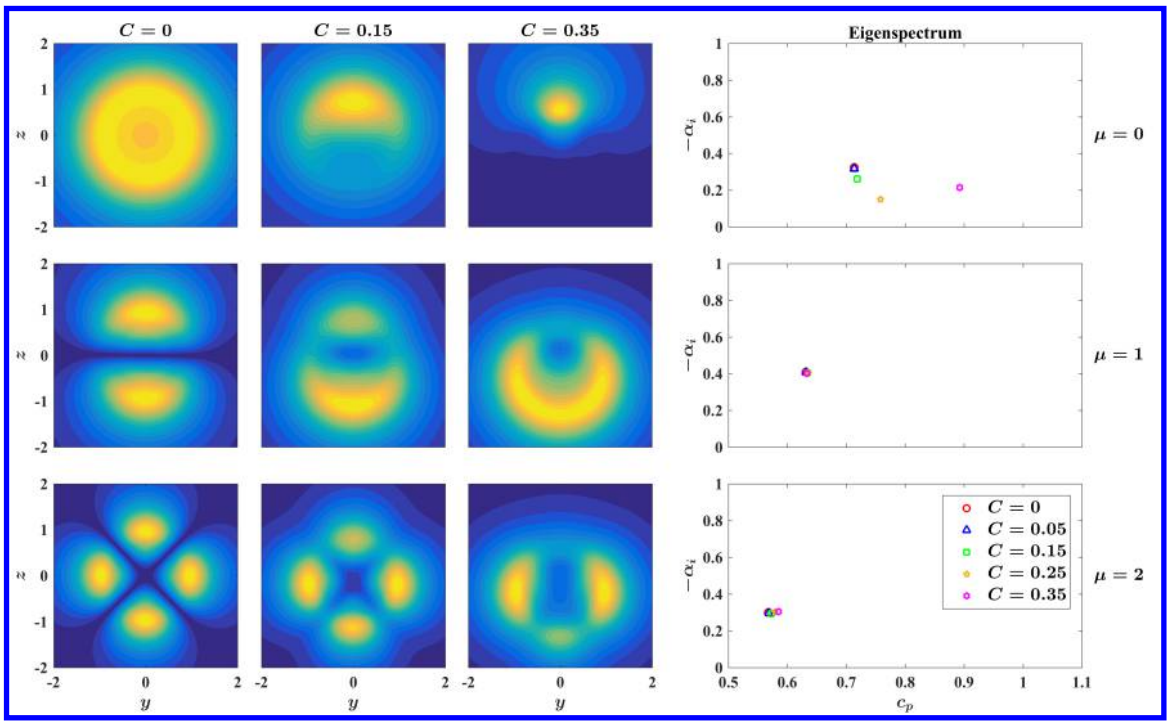

(b) Outer modes at $x = 4$.

Figure 3: Outer mode LST eigensolutions for $St = 0.1$ following the scheme of fig. 2.

of the jet, there is a consistent decrease of growth rate in all cases (except for the $\mu = 2$ outer mode in the fully eccentric jet). Except for the $\mu = 0$ inner modes, we also note a decrease in phase speed, which is more pronounced in the outer modes. This decrease is linked to the diminished radiative efficiency of the associated wavepackets[18]. Several modes become stable by $x = 5$; this would have happened at earlier

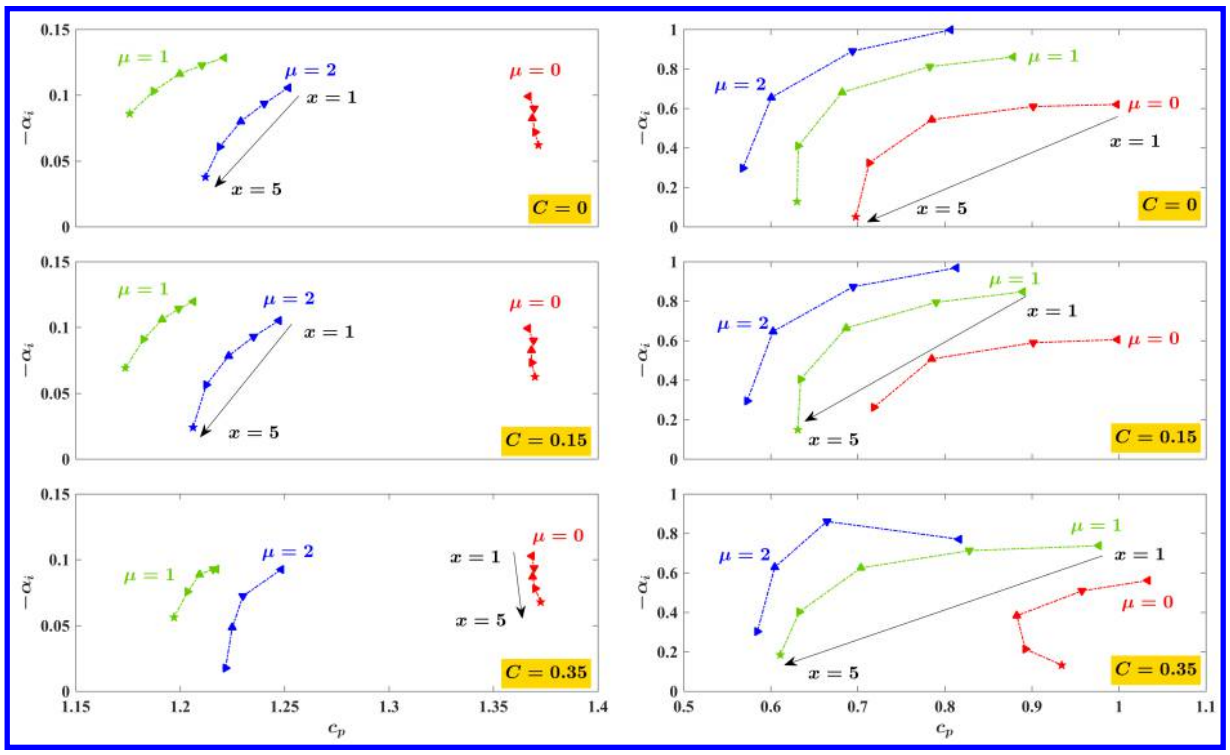

(a) Inner modes (b) Outer modes

Figure 4: LST eigenvalues of (a) inner and (b) outer modes of $St = 0.1$ for coaxial jet (top row), partial offset jet (middle row) and fully eccentric jet (bottom row). In each case, results are presented for the first three μ modes (viz. $\mu = 0$, 1 and 2) at five x-stations (viz. $x = 1$, 2, 3, 4 and 5); however, the display of modes is omitted for $x = 5$ (pentagram marker) if they are stable thereat.

$x-$stations if a higher Strouhal number were considered.

Further explication of the effect of jet eccentricity on the azimuthal directivity of the noise-producing wavepackets may be found in the composite LST eigenfunctions presented in fig. 5. It will be recalled from eqn. (6) that these are obtained by integrating the normalized eigensolutions over an axial range. The preferential diminution of the wavepackets of the $\mu = 1$ and 2 inner modes in the bottom sector with increasing jet offset becomes apparent in this perspective. The $\mu = 0$ inner mode, on the other hand, appears substantially unaffected by jet eccentricity. As an aside, we estimate the wavelength of these inner mode wavepackets to be about $8D_p$ at the $St = 0.1$ studied, since we have captured about half of the cycle in an axial span of $4D_p$.

The outer modes show a reversal of behaviour. Namely, the $\mu = 0$ outer mode gets severely diminished in the bottom sector in the fully eccentric jet, whereas the $\mu = 1$ and 2 outer modes appear strengthened thereat. As mentioned previously, we expect the contribution of the outer modes to far-field noise to be small in actual jet engines. The wavelength of the outer mode wavepackets is approximately $4D_p$ at $St = 0.1$.

One should not be confused by the relative radial extents of the inner and outer wavepackets observed in fig. 5. They have widely disparate strengths close to the nozzle exit, which is simply an artifact of their similar strengths at the end of the integration domain. A fairer comparison will involve equalizing the initial strengths of the modes, in keeping with the empirically-observed flat spectrum of disturbances in the shear layer at the nozzle exit; however, this was not pursued here.

V. Conclusion

In an effort at reduction of effective noise from dual-stream jets, it has been proposed previously to offset the secondary stream with respect to the primary stream such that the thicker shear layer is oriented below

Downloaded by Aniruddha Sinha on June 28, 2018 | http://arc.aiaa.org | DOI: 10.2514/6.2018-3941

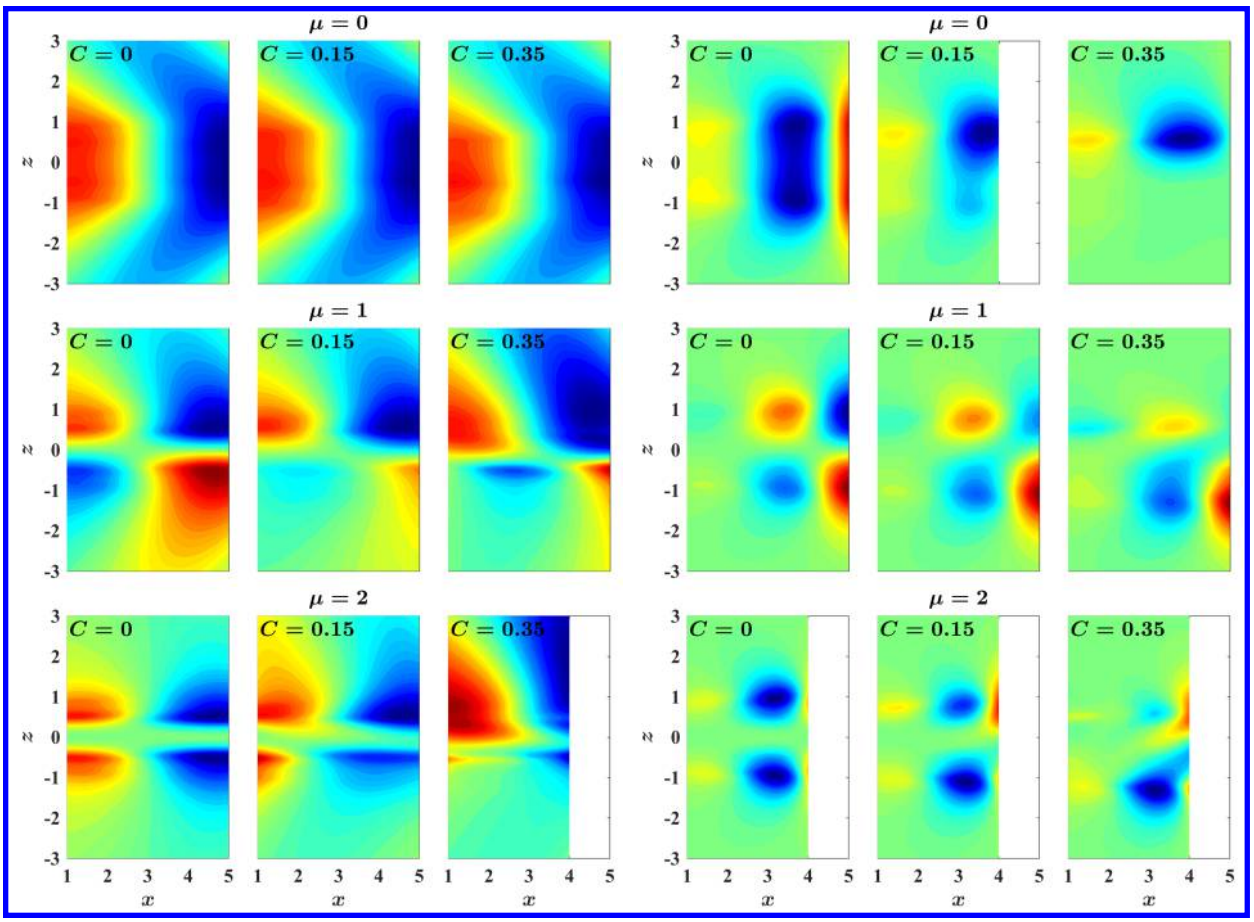

(a) Inner modes (b) Outer modes

Figure 5: Real part of pressure component from composite LST eigenfunctions of (a) inner, and (b) outer modes for $St = 0.1$ in coaxial jet (left column), partial offset jet (center column) and fully eccentric jet (right column). Results for $\mu = 0$, 1 and 2 are presented in the top, middle and bottom rows, respectively. The integration is stopped at $x = 4$ for those modes that get stabilized by $x = 5$. The colorscales for all plots go from -1 (blue) to $+1$ (red), with 0 being light green.

the jet. Experiments have shown that this can reduce the noise radiation to the bottom sector, which is beneficial for ground personnel as well as built structures.

In this paper we investigate the linear stability of a series of two-stream jets having increasing offset, with the goal of predicting the modification of the hydrodynamic noise sources in line with the trends observed in experiments. To this end, we first propose a modelling approach for the mean axial velocity field that is uniformly valid across the possible range of offsets. Our model is informed by the sparse experimental data reported in Ref. 5. However, this database also limits the study to jets with relatively high-speed secondary streams (Mach 0.9).

To aid in the conceptual understanding of the stability characteristics, the bi-global quasi-parallel stability problem is solved in the Fourier azimuthal domain. From this, we extract eigensolutions that are dominated by azimuthal modes 0, 1 and 2 (axisymmetric mode, and first and second helical modes). These low-order azimuthal modes dominate the far-field acoustics in high-speed jets due to their strong coherence [37,38].

The LST results indicate that the acoustically-efficient inner eigensolutions associated with the primary shear layer become preferentially less dominant in the thickened shear layer below the jet with increasing eccentricity. In particular, although the inner mode dominated by the axisymmetric mode does not display any strong azimuthal directivity, the inner modes dominated by the first and second helical modes display significant weakening below the jet. This may be the root cause of the observed azimuthal directivity of

Downloaded by Aniruddha Sinha on June 28, 2018 | http://arc.aiaa.org | DOI: 10.2514/6.2018-3941

offset jets.

The outer eigensolutions associated with the secondary shear layer present the opposite trend. Specifically, the predominantly-axisymmetric outer mode is strongly biased towards the top of the jet, whereas the outer modes dominated by the first and second helical modes display a preference for the bottom of the jet. We expect the outer modes to be of lower importance in practical jets where the secondary stream is significantly slower and colder than the primary stream.

The current study was limited to a Strouhal number of 0.1 (normalized by inner jet parameters). In the future, we will analyze higher Strouhal numbers (around 0.3) that are more strongly implicated in far-field radiation. We will also study two-stream jets with varying velocity ratios to understand the relative importance of the inner and outer modes. Finally, the quasi-parallel assumption of LST may be relaxed somewhat in the future to better account for the streamwise development of the jet.

Acknowledgements: AS acknowledges support from Industrial Research and Consultancy Center of Indian Institute of Technology Bombay, via the seed grant program.

References

[1] M. J. Lighthill. On sound generated aerodynamically. I. General theory. *Proc. R. Soc. Lond. A*, 211(1107):564–587, 1952.
[2] K. Viswanathan. Parametric study of noise from dual-stream nozzles. *Journal of Fluid Mechanics*, 521:35–68, 2004.
[3] C. E. Tinney and P. Jordan. The near pressure field of co-axial subsonic jets. *Journal of Fluid Mechanics*, 611:175–204, 2008.
[4] D. Papamoschou and S. Rostamimonjezi. Effect of velocity ratio on noise source distribution of coaxial jets. *AIAA Journal*, 48(7):1504–1512, 2010.
[5] E. Murakami and D. Papamoschou. Mean flow development in dual-stream compressible jets. *AIAA Journal*, 40(6): 1131–1137, 2002.
[6] D. Papamoschou. New method for jet noise reduction in turbofan engines. *AIAA Journal*, 42(11):2245–2253, 2004.
[7] D. Papamoschou. Fan flow deflection in simulated turbofan exhaust. *AIAA Journal*, 44(12):3088–3097, 2006.
[8] C. A. Brown, J. E. Bridges, and B. Henderson. Offset stream technology test – summary of results. In *13th AIAA/CEAS Aeroacoustics Conference, AIAA Paper 3664*, 2007.
[9] D. Papamoschou, A. D. Johnson, and V. Phong. Aeroacoustics of three-stream high-speed jets from coaxial and asymmetric nozzles. *Journal of Propulsion and power*, 30(4):1055–1069, 2014.
[10] D. Papamoschou, V. Phong, J. Xiong, and F. Liu. Quiet nozzle concepts for three-stream jets. In *54th AIAA Aerospace Sciences Meeting, AIAA Paper 523*, 2016.
[11] B. Henderson, S. J. Leib, and M. P. Wernet. Measurements and predictions of the noise from three-stream jets. In *21st AIAA/CEAS Aeroacoustics Conference, AIAA Paper 3120*, 2015.
[12] B. Henderson and D. L. Huff. The aeroacoustics of offset three-stream jets for future commercial supersonic aircraft. In *22nd AIAA/CEAS Aeroacoustics Conference, AIAA Paper 2992*, 2016.
[13] B. Henderson and M. P. Wernet. Characterization of three-stream jet flow fields. In *54th AIAA Aerospace Sciences Meeting, AIAA Paper 1636*, 2016.
[14] N. J. Georgiadis, D. A. Yoder, and W. A. Engblom. Evaluation of modified two-equation turbulence models for jet flow predictions. In *44th AIAA Aerospace Sciences Meeting and Exhibit, AIAA Paper 0490*, 2006.
[15] V. Dippold III, L. Foster, and M. Wiese. Computational analyses of offset-stream nozzles for noise reduction. *Journal of Propulsion and Power*, 25(1):204–217, 2009.
[16] J. Xiong, P. Nielsen, F. Liu, and D. Papamoschou. Computation of high-speed coaxial jets with fan flow deflection. *AIAA Journal*, 48(10):2249–2262, 2010.
[17] D. Papamoschou and S. Rostamimonjezi. Modeling of noise reduction for turbulent jets with induced asymmetry. In *18th AIAA/CEAS Aeroacoustics Conference, AIAA Paper 2158*, 2012.
[18] P. Jordan and T. Colonius. Wave packets and turbulent jet noise. *Annu. Rev. Fluid Mech.*, 45:173–195, 2013.
[19] E. Mollo-Christensen. Measurements of near field pressure of subsonic jets. Technical report, NATO A. G. A. R. D. Report 449, 1963.
[20] D. G. Crighton and M. Gaster. Stability of slowly diverging jet flow. *Journal of Fluid Mechanics*, 77(2):397–413, 1976.
[21] C. K. W. Tam and D. E. Burton. Sound generated by instability waves of supersonic flows. Part 2. Axisymmetric jets. *Journal of Fluid Mechanics*, 138:273–295, 1984.
[22] T. Suzuki and T. Colonius. Instability waves in a subsonic round jet detected using a near-field phased microphone array. *Journal of Fluid Mechanics*, 565:197–226, 2006.
[23] K. Gudmundsson and T. Colonius. Instability wave models for the near-field fluctuations of turbulent jets. *Journal of Fluid Mechanics*, 689:97–128, 2011.
[24] A. Sinha, D. Rodríguez, G. Brès, and T. Colonius. Wavepacket models for supersonic jet noise. *Journal of Fluid Mechanics*, 742:71–95, 2014.
[25] M. D. Dahl and P. J. Morris. Noise from supersonic coaxial jets. Part 2: Normal velocity profile. *Journal of Sound and Vibration*, 200(5):665–699, 1997.
[26] D. Perrault-Joncas and S. A. Maslowe. Linear stability of a compressible coaxial jet with continuous velocity and temperature profiles. *Physics of Fluids*, 20:074102, 2008.
[27] M. Gloor, D. Obrist, and L. Kleiser. Linear stability and acoustic characteristics of compressible, viscous, subsonic coaxial jet flow. *Physics of Fluids*, 25:084102, 2013.

Downloaded by Aniruddha Sinha on June 28, 2018 | http://arc.aiaa.org | DOI: 10.2514/6.2018-3941

[28] G. Balestra, M. Gloor, and L. Kleiser. Absolute and convective instabilities of heated coaxial jet flow. *Physics of Fluids*, 27 (5):054101, 2015.
[29] A. Sinha, D. V. Gaitonde, and N. Sohoni. Parabolized stability analysis of dual-stream jets. In *22nd AIAA/CEAS Aeroacoustics Conference, AIAA Paper 3057*, 2016.
[30] A. Towne and T. Colonius. One-way spatial integration of hyperbolic equations. *Journal of Computational Physics*, 300: 844–861, 2015.
[31] T. R. Troutt and D. K. McLaughlin. Experiments on the flow and acoustic properties of a moderate-Reynolds-number supersonic jet. *Journal of Fluid Mechanics*, 116:123–156, 1982.
[32] M. R. Khorrami and M. R. Malik. Efficient computation of spatial eigenvalues for hydrodynamic stability analysis. *Journal of Computational Physics*, 104(1):267–272, 1993.
[33] F. Li and M. R. Malik. Spectral analysis of parabolized stability equations. *Computers & Fluids*, 26(3):279–297, 1997.
[34] K. Mohseni and T. Colonius. Numerical treatment of polar coordinate singularities. *Journal of Computational Physics*, 157:787–795, 2000.
[35] K. W. Thompson. Time dependent boundary conditions for hyperbolic systems. *Journal of Computational Physics*, 68: 1–24, 1987.
[36] R. B. Lehoucq, D. C. Sorensen, and C. Yang. *ARPACK users' guide: solution of large-scale eigenvalue problems with implicitly restarted Arnoldi methods*. SIAM, 1998.
[37] D. Juvé, M. Sunyach, and G. Comte-Bellot. Filtered azimuthal correlations in the acoustic far field of a subsonic jet. *AIAA Journal*, 17(1):112–113, 1979.
[38] A. V. G. Cavalieri, G. Daviller, P. Comte, P. Jordan, G. Tadmor, and Y. Gervais. Using large eddy simulation to explore sound-source mechanisms in jets. *Journal of Sound and Vibration*, 330(17):4098–4113, 2011.

Downloaded by Aniruddha Sinha on June 28, 2018 | http://arc.aiaa.org | DOI: 10.2514/6.2018-3941